Computational Methods Enable the Prediction of Improved Catalysts for Nickel-Catalyzed Cross-Electrophile Coupling

Michelle E. Akana[†], Sergei Tcyrulnikov[‡], Brett D. Akana-Schneider[†], Giselle P. Reyes[‡], Sebastien Monfette[‡], Matthew S. Sigman[§*], Eric C. Hansen[‡*], and Daniel J. Weix[†*]

[†]Department of Chemistry, University of Wisconsin-Madison, Madison, WI 53706, United States

[‡]Chemical Research and Development, Pfizer Worldwide Research and Development, Groton, CT 06340, United States

[§]Department of Chemistry, University of Utah, Salt Lake City, UT 84112, United States

Supporting Information Placeholder

ABSTRACT: Cross-electrophile coupling has emerged as an attractive and efficient method for the synthesis of C(sp^2)–C(sp^3) bonds. These reactions are most often catalyzed by nickel complexes of nitrogenous ligands, especially 2,2'-bipyridines. Precise prediction, selection, and design of optimal ligands remains challenging, despite significant increases in reaction scope and mechanistic understanding. Molecular parameterization and statistical modeling provide a path to the development of improved bipyridine ligands that will enhance the selectivity of existing reactions and broaden the scope of electrophiles that can be coupled. Herein, we describe the generation of a computational ligand library, correlation of observed reaction outcomes with features of the ligands, and in silico design of improved bipyridine ligands for Ni-catalyzed cross-electrophile coupling. The new nitrogen-substituted ligands display a fivefold increase in selectivity for product formation versus homodimerization when compared to the current state of the art. This increase in selectivity and yield was general for several cross-electrophile couplings, including the challenging coupling of an aryl chloride with an *N*-alkylpyridinium salt.

Introduction

Heterocycle-based, L2 dinitrogen ligands are critical enabling components of many transition metal-catalyzed C–C, C–N, and C–O bond forming reactions. These ligands—typified by 2,2'-bipyridine (bpy)—enable reactivity distinct from phosphine ligands by promoting a diverse set of 1- and 2-electron-processes.[1–4] In particular, bpy ligands have become a fixture of nickel-catalyzed cross-electrophile,[5] metallophotoredox,[6] and electrochemical[7–9] couplings, and are often the standard by which the reactivity of other ligands are gauged. The increased demand for more diverse bipyridine ligands can be observed in the surge of interest in substituted bipyridines (Figure 1A, Figure S1.1). Despite this diversification and their impact on numerous fields, few studies have systematically examined what molecular features are critical to success in this class of ligands.

As a prominent example, Ni-catalyzed C(sp^2)-C(sp^3) cross-electrophile coupling (XEC)[10–12] is dependent on the selection of an appropriate ligand, most often a bpy derivative. While extensive optimization and expansion of this reaction manifold has enabled the use of new substrate classes, dimerization of the C(sp^2) component remains problematic. Slow radical capture can allow competitive aryl exchange of the intermediate arylnickel(II) species to compete (Figure 1B).[13,14] Approaches to mitigate this issue often focus on either increasing the rate of radical generation—in an effort to accelerate the productive pathway—or decreasing the rate of disproportionation of the arylnickel intermediate.

Methods from Weix,[15–17] Sevov,[18] and others[12,19–21] have demonstrated the use of multimetallic catalyst systems where one catalyst is exclusively responsible for generation of an alkyl radical, and another engages the C(sp^2) coupling partner and facilitates formation of the desired C–C bond (Figure 1C, part i).[22,23] An alternative approach is the addition of stoichiometric additives—such as phthalimide or pyridine derivatives—that passivate open sites of the arylnickel intermediate, slowing the rate of deleterious disproportionation (Figure 1C, part ii).[12,24–26] While these and other modifications have proven effective in many cases, they also introduce complications—such as tuning catalyst ratios, decreased atom economy, and new side reactions. A more attractive approach would be the systematic development of a more selective single catalyst. Further, improved catalysts could be used in combination with the above methods to improve rate or engage otherwise inaccessible substrate pools.

The underlying issue to this approach is that the discovery of nitrogen-based ligands is less well developed than phosphines. This is reflected in the disparity in commercial availability and the prevalence of novel ligands in the literature. Thus far, approaches to overcome this developmental gap have focused on general surveys of reactivity,[2,27] hypothesis-driven skeletal modifications,[28] or high-throughput experimentation (HTE) campaigns to identify new classes of ligands,[29] often with the goal of expanding reaction scope to access more challenging substrates. More frequently, HTE is employed to identify an optimal catalyst from a pre-existing suite of ligands with validated reactivity.[30,31] While these methods have provided a basis of understanding for the reactivity of specific catalysts, they have yet to deliver a sufficiently detailed model of reactivity to enable the design of improved ligands.

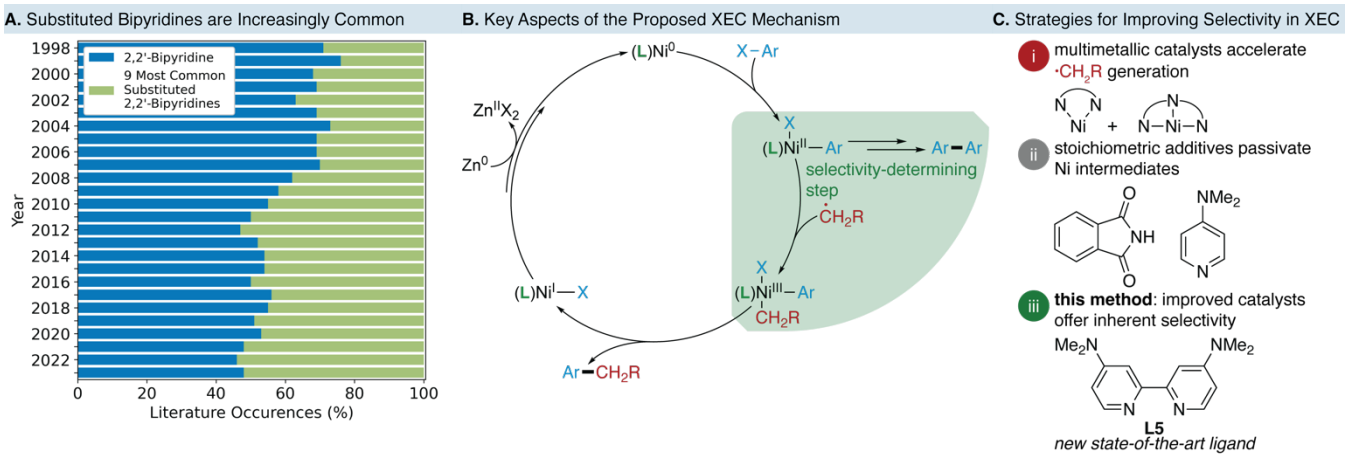

Figure 1. Bipyridines Are Critical to Cross-Electrophile Coupling, But Further Improvements Are Needed. (A) Occurrences and prevalence of 2,2'-bipyridine ligands were gathered from a Reaxys structure search performed on 6/28/23 for 2,2'-bipyridine with attached GH groups in each available position. The results were filtered to exclude higher order polypyridines and compounds most utilized in organic light emitting diodes (MW > 500 g/mol). For additional information concerning the identity and total occurences of various bipyridines since 1973, see section 1.3 of the Supporting Information (B) Slow radical capture can enable undesired side pathways in nickel-catalyzed cross electrophile coupling (XEC). (C) Common strategies to improve selectivity in XEC include the use of additional catalysts that accelerate radical generation and the addition of stoichiometric additives that de crease the rate of decomposition of the (L)Ni^{II}(Ar)X intermediate.

In this context, statistical methods that correlate computationally-derived molecular features to reaction outcomes have accelerated the design, selection, and commercialization of optimal phosphine-ligated catalysts.[32–34] Thus far, the translation of these methods to L2 dinitrogen ligands remains limited. Most often, the resulting statistical models are utilized to rationalize enantio- or site-selectivity. For example, the Sigman group has reported the use of multivariate linear regression to rationalize and design improved 2-(2-pyridyl)oxazoline ligands in enantioselective Heck arylations.[35,36] Additionally, Doyle and coworkers have utilized a similar workflow to explain the improved enantioselectivity provided by 2,2'-biimidazoline ligands compared to related bioxazolines—specifically exploring correlations with descriptors from (L)Ni(F)$_2$ and (L)Ni(Ar)Cl complexes—where they noted improved correlations when parameters were sourced directly from the catalytic intermediate involved in the stereodetermining step.[37] Based on the general success of these approaches, we hypothesized that a similar data science workflow could be applied to more general obstacles of selectivity in nickel-catalyzed cross-electrophile couplings.

Herein, we describe the application of modern computational and statistical methods to construct correlations of reaction performance in cross-electrophile couplings as a function of the bipyridine ligand. The resulting models communicate two key features of a successful catalyst: a square planar (L)Ni^{II}(Ar)Br intermediate and a strongly donating ligand. This model is robust and predictive, allowing for the interpolative and extrapolative prediction of performance for untested bipyridine ligands. Additionally, we designed a suite of improved 4,4'-bis(dialkylamino)-2,2'-bipyridine ligands in silico, which were predicted to provide significant improvements in selectivity for the desired product. In action, these new ligands facilitate the high yielding coupling of a variety of alkyl and aryl electrophiles. We expect that the expanded application of the improved ligands identified in this study will enable the accelerated development of new cross-coupling reactions.

Results and Discussion

We initially selected the cross-electrophile coupling of primary alkyl bromides with aryl bromides as a model reaction for studying the impact of ligand structure on reaction performance (Figure 1A). This validated coupling has been used as a model system in several ligand identification studies and for the translation of XEC methods to other reductive systems.[29,38] The yield is generally limited by the formation of byproducts—primarily the aryl homodimer (**4**)—and selectivity is determined by the relative concentrations of **3** to **4** at 24 h. The ratio of product to aryl homodimer can be expressed as a difference in activation energy, $\Delta\Delta G^{\ddagger}$, via the Curtin-Hammett equation, $\Delta\Delta G^{\ddagger} = -RT\ln([\mathbf{3}]/[\mathbf{4}])$. As such, negative values of $\Delta\Delta G^{\ddagger}$ are obtained for reactions that selectively form product **3** over dimer **4.**

We gathered an initial dataset by screening a suite of substituted bipyridines and related ligands in 96-well plates on 20 µmol scale. This ligand suite resulted in a wide dynamic range of results (2–82% yield of **3** over a range of 3.51 kcal/mol in $\Delta\Delta G^{\ddagger}$, Figure S4.1) and confirmed that the yield of the desired product is primarily determined by the selectivity for the cross-product (**3**) over the aryl homodimer (**4**) (Figure S4.2).

Given the diversity in substitution patterns in the bpy ligands tested (4,4'-, 5,5'-, 6-, or 6,6'-(di)substituted), it was readily apparent that tabulated molecular descriptors (i.e., Hammett or Charton values) would be insufficient for modelling selectivity (Figure S5.15). To gain insight into the intrinsic characteristics of each catalyst and adequately describe this diversity, we generated a library of DFT-optimized (L)Ni^{II}(Ph)Br (Figure 1A) complexes from which we would derive molecular parameters.[39–47]

We hypothesized that parameters derived directly from the oxidative addition complex—the intermediate that is responsible for defining selectivity—would provide unique insight into the structure of selective catalysts.[37] Further, the resulting dataset should be translatable to other nickel-catalyzed cross-couplings of haloarenes. We obtained a variety of electronic (e.g., Natural Population Analysis (*NPA*) charges of atoms in the primary coordination sphere, nickel d-orbital energies and

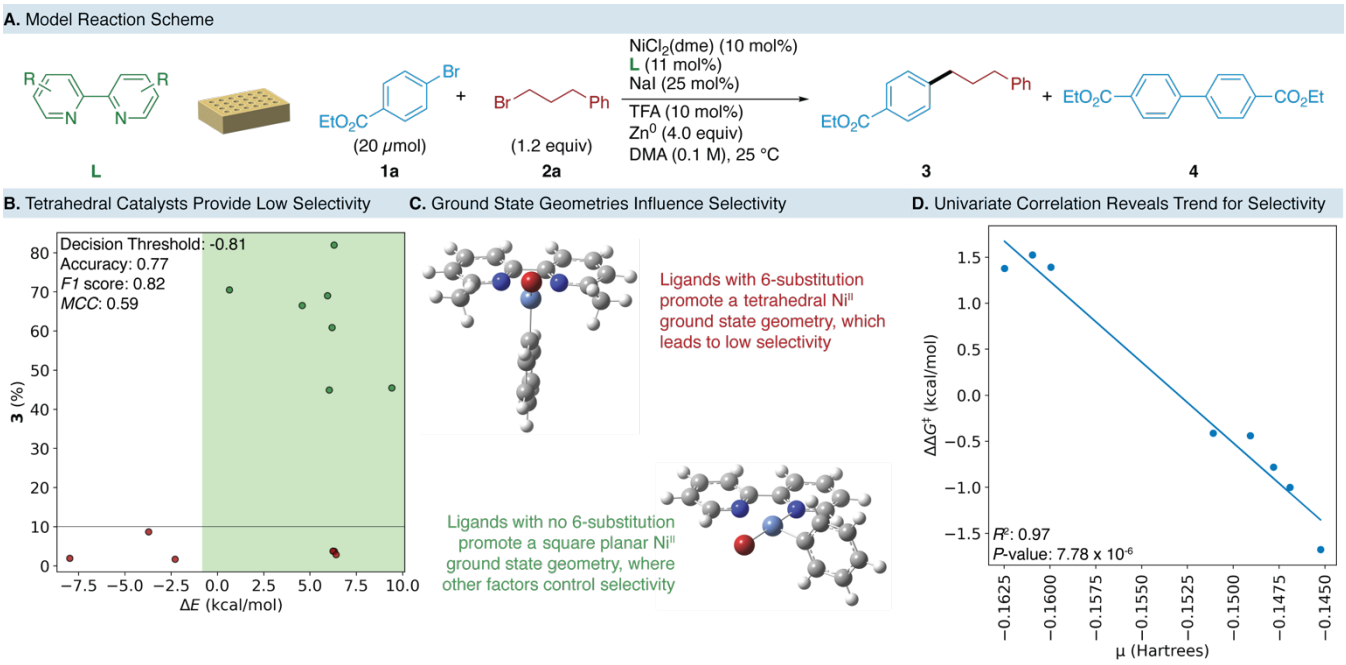

Figure 1. Model Reaction and Initial Insights into the Source of Selectivity. (A) The selectivity of a model XEC reaction is determined by the bipyridine ligand employed. For the results of all ligands evaluated, see Figures S2.1 and S4.1. (B) Classification of reaction yields reveals that ligands that adopt a tetrahedral geometry in the ground state provide low yield and selectivity. ΔE = E(tetrahedral) – E(square planar), where negative values indicate ground state tetrahedral complexes. For additional information on threshold analysis, see Section 5.3 of the Supporting Information. (C) Representative geometries promoted by ligands with (top) and without (bottom) substitution in the 6 position. (D) Strong univariate correlations indicate that electron-rich ligands (bottom right) provide improved selectivity over electron-poor ligands (top left). Chemical potential (μ) provides a strong and robust model for the selectivity promoted by symmetrically substituted bipyridine catalysts. Selectivity is represented by $\Delta\Delta G^{\ddagger}$, where negative values of $\Delta\Delta G^{\ddagger}$ represent reactions that are more selective for **3** over **4**.

occupancies, etc.) and steric parameters for each catalyst in both the square planar and tetrahedral geometry.[48] This computational dataset offers detailed insight into the electronic and steric structure of each catalyst and is provided in full as a supplementary file.

Initial linear correlations between the experimental results and computational descriptors yielded poor results that did not adequately incorporate a grouping of observations that gave ≤1 turnover to form **3** (10% yield). We hypothesized that two separate features may lead to low selectivity via distinct mechanisms. Indeed, classification of yield of **3** using a single node decision tree with a threshold value of 10% yield revealed a reactivity cliff based on the difference in energy between the tetrahedral and square planar geometries of the (L)Niᴵᴵ(Ph)Br complex (Figure 1B).[49] Sterically hindered 6- and 6,6'-(di)substituted ligands promote a tetrahedral geometry in the ground state and rapidly dimerize the aryl bromide, leading to low selectivity. Contrastingly, ligands with 4,4'- or 5,5'-subsitition yield (L)Niᴵᴵ(Ph)Br complexes with a square planar ground state and tended to result in yields >10% of **3** across a range of selectivities.

Bipyridine ligands with 6,6'-disubstitution and related phenanthrolines are known to display reactivity distinct from their unhindered analogues (Figure 1C).[50,51] We do not believe that this is a result of disfavoring polyligated nickel complexes (e.g., $(L)Ni^{II}(X)_2$, $(L)_2Ni^{II}(X)_2$, and $[(L)_3Ni^{II}]X_2$), as bipyridines with large 5,5'-substituents—which display reliable monoligation—provide similar reactivity to unhindered bpys.[28] Instead, it appears that these ligands' promotion of a triplet, tetrahedral ground state geometry plays a decisive role in acceleration of the formation of the aryl homodimer **4**.

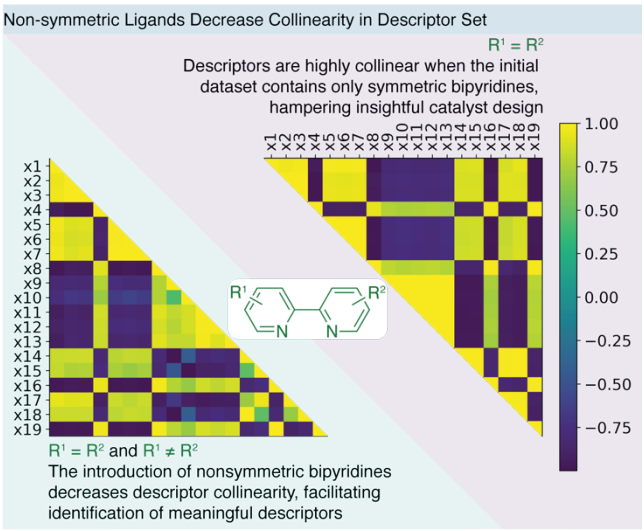

Figure 2. Excessive Collinearity in the Descriptor Set of Symmetric Ligands Can Be Resolved With Non-Symmetric Ligands. Amongst the 19 strong correlations (R2> 0.7, p-value < 0.01) identified using only symmetric ligands, there was a high degree of collinearity (indicated by bright yellow and dark indigo in the collinearity matrix on the right). The introduction of 3 non-symmetric ligands decreased the number of strong correlations (10 examples where R2 > 0.7 and only 3 where R2 > 0.9) and lowered collinearity (seen in the matrix on the left using the same 19 parameters). The identity and statistical measures of each correlation is provided in Section 5 of the Supporting Information.

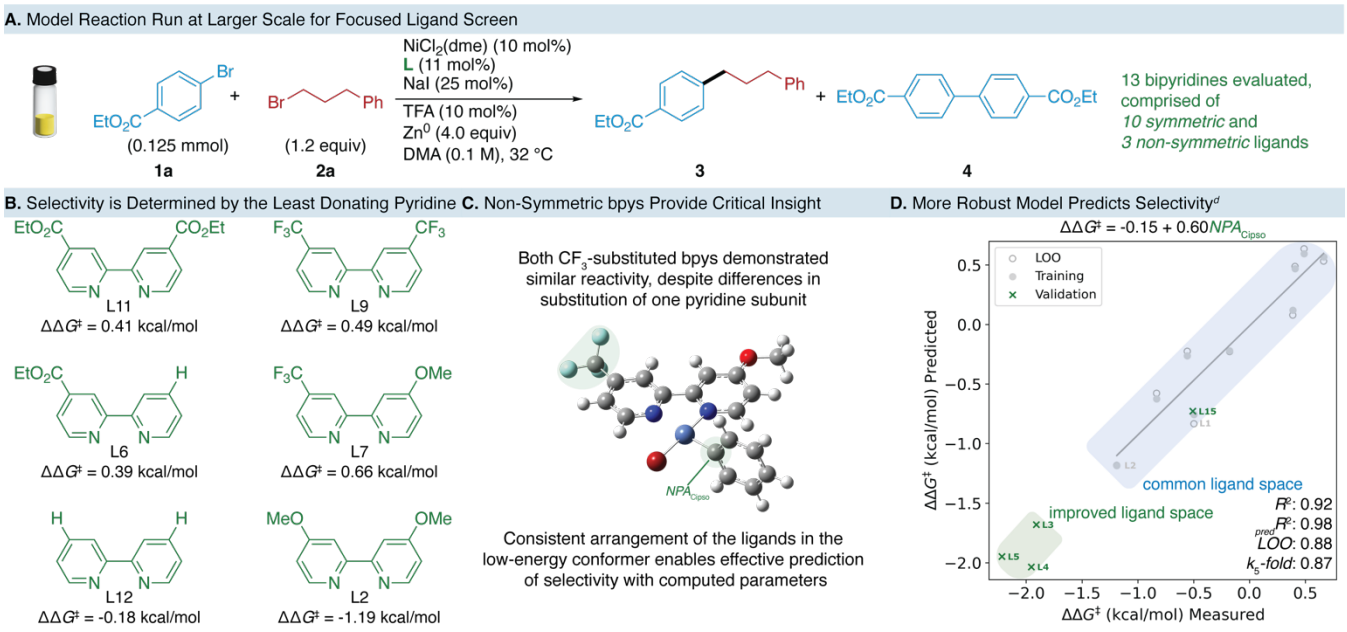

Figure 3. A Tailored Dataset Enables a More Robust Model. (A) A selection of symmetrically and non-symmetrically 4,4'-disubstituted ligands were evaluated on a larger scale to confirm and expand on previous results. For the results of all ligands evaluated, see Figures S2.1 and S4.3. (B) Non-symmetrically substituted ligands provide selectivity based on the least electron-dense pyridine donor. The observed selectivity for each ligand is provided. (C) The phenyl ligand is consistently trans to the least donating pyridine ring in the low energy square planar isomer. This arrangement allows the Natural Population Analysis charge of the ipso carbon (NPA_{Cipso}) to correlate strongly with selectivity. (D) A robust and predictive model for selectivity was found based on NPA_{Cipso}. MAE for the training and validation sets are 0.15 and 0.20, respectively. For more information on the optimal and alternative models, see Figure S5.11.

A training set limited to 4,4'- and 5,5'-disubstituted bipyridines yielded several significant (R^2 > 0.7 and p-value < 0.01) univariate correlations between molecular descriptors and selectivity (Figure 1D and Figure S5.7). The best correlations directly utilized the frontier molecular orbital energies, or arithmetic combinations thereof. Amongst these correlations we found a robust (R^2, *LOO*, and k_5-*fold* all > 0.9., Figure S5.9) univariate model for selectivity based on μ. As the average of the HOMO and LUMO energies, μ increases with increased donation of the ligand. This is reflected in the qualitative trend that ligands bearing electron-donating ligands in the 4,4'-positions yielded the highest selectivity.

Despite this initial success, the specificity and translatability of the μ model remained unclear. We found that the best univariate correlations (19 examples where R^2 > 0.70 and p-value < 0.01) existed between directionally oriented, highly collinear descriptors (Figure 3, Figure S5.8). The collinearity in the parameters caused by the symmetric bipyridine structures led to convolution of the computational dataset. As such, we hypothesized that the introduction of non-symmetrically substituted bipyridines would serve to decrease the number of collinear directional descriptors and differentiate directional or atom-specific descriptors (e.g., *NPA* charge of a single nitrogen donor) from additive parameters (e.g., μ). To test this hypothesis, we constructed a suite of non-symmetric and select symmetrically substituted bpys, which were subsequently evaluated on a larger scale (0.125 mmol, Figure 3A).

Univariate correlations utilizing this new dataset revealed that many of the strong correlations that we had previously observed were not maintained with the introduction of non-symmetric ligands (10 examples where R^2 > 0.7, Figure S5.10). In fact, the previous best correlation involving μ was significantly weakened (R^2 of the univariate correlation decreased from 0.97 to 0.75, Figure S5.12). This is due to selectivity being solely determined by the least donating pyridine unit; for example, 4-methoxy-4'-(trifluoromethyl)-2,2'-bipyridine (**L8**) yields selectivity similar to 4,4'-bis(trifluoromethyl)2,2'-bipyridine (**L9**), rather than 4,4'-dimethoxy-2,2'-bipyridine (**L2**) (ΔΔG‡ = 0.66, 0.49, and -1.19 respectively, Figure 4B, Figure S4.3).

Using these results, we identified a more robust univariate correlation based upon the *NPA* charge of the phenyl C_{ipso} (Figure 3D). This model was then used to predict the performance of several ligands with the goal of both validating the model and finding better catalysts (vide infra). We observed that this model was enabled by the consistent alignment of the least electron-rich pyridine ring—which determines selectivity—trans to the phenyl ligand in the lowest-energy isomer (Figure 4C).[52,53] As the nitrogen trans to C_{ipso} becomes more donating, the *NPA* charge of C_{ipso} decreases, and selectivity rises.

This model is robust—*LOO* = 0.88, k_5-*fold* = 0.87—and predictive ($_{pred}R^2$ = 0.98) of both an interpolated and extrapolated observations. The use of computational parameters derived directly from a catalytic intermediate offers a distinct advantage over the use of tabulated descriptors—such as Hammett parameters. First, the model effectively predicts the selectivity of 5,5'-disubstituted bpy derivatives, as DFT gauges π-donation across the bpy backbone. Second, the model accurately predicted the selectivity of non-symmetrically substituted ligands without direct intervention; this is mainly attributable to the consistent orientation of the donor atoms in the low energy isomer. Further, the specificity of DFT-derived parameters can provide more impactful mechanistic insight.

Table 1. Ligands Designed In Silico Outperform State-of-the-art Bipyridines[a]

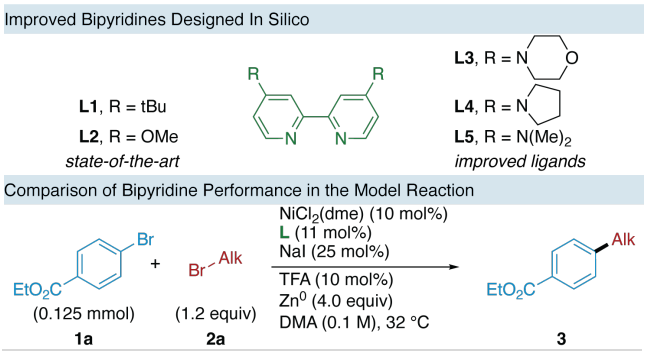

entry	L	yield **3** (%)	selectivity (**3**:**4**)	NPA_{Cipso} (*e*)	$\Delta\Delta G^{\ddagger}$ (kcal/mol)[b]
1	L1	49	2:1	-0.1519	-0.5
2	L2	61	7:1	-0.1530	-1.19
3	L3	82	23:1	-0.1543	-1.91
4	L4	88	25:1	-0.1552	-1.95
5	L5	79	39:1	-0.1550	-2.22

[a]Alk = 3-Phenylpropyl. Reactions were assembled in a nitrogen filled glovebox in 1.25 mL of DMA. Yields determined by GC. [b]Listed $\Delta\Delta G^{\ddagger}$ are those observed experimentally and are consistent with the predicted values, as seen in Figure 3D.

Despite this model's accuracy in predicting the selectivity provided by various ligands, it is still unclear by what pathway **4** forms. Direct disproportionation of (L)Ni^{II}(Ar)Br,[54] zinc-mediated transfer between two (L)Ni^{II}(Ar)Br complexes,[55,56] and reduction followed by a second oxidative addition[57–59] are all precedented for biaryl formation from arylnickel(II) species. Our data is inconsistent with both direct disproportionation[60] and sequential oxidative addition[61], but consistent with zinc-mediated aryl transfer (Figure S4.9).[62] Further experiments are needed to firmly establish the exact mechanism of biaryl formation, but are beyond the scope of this publication.

Via extrapolation from the model, we predicted the selectivity promoted by a series of improved 4,4'-bis(dialkylamino)-2,2'-bipyridines in silico (Table 1). After synthesizing these ligands, we found that the model had correctly predicted the over fivefold increase in selectivity that they enabled (from 7:1 to 39:1 **3**:**4** for **L2** and **L5** respectively). To investigate the generality of these improved bipyridine ligands, we benchmarked them in the cross-electrophile coupling of a variety of aryl and alkyl halide pairings. We found that both the overall and relative selectivity significantly improved when coupling less reactive and more abundant chloroarenes (Table 2, entry 1). We noted an increase in selectivity was also observed when coupling more reactive iodoarenes (Table 2, entry 3). This improvement is due to the production of stoichiometric iodide as a byproduct of the reaction (Table 2, entry 2, Figure S4.6). **L5** provided improvements in selectivity compared to **L2** in the coupling of bromoarenes regardless of the electron-density of the substrate (Table 2, entries 4 and 5, Figure S4.8). Given the similar mechanisms proposed for a variety of XEC reactions, **L5** may be useful for improving and extending the scope of many reactions of this type.

Table 2. Benchmarking of Bipyridine L5 in the XEC of Aryl Halides with Alkyl Bromides[a]

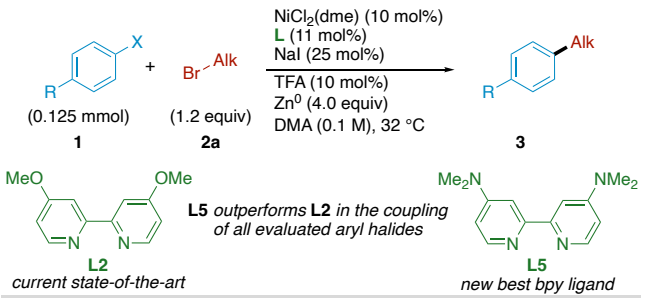

entry	X	R	result with **L5** (yield **3**(%), **3**:**4**)	result with **L2** (yield **3**(%), **3**:**4**)
1	Cl	CO_2Et	93, 311:1	85, 17:1
2	Br	CO_2Et	79, 39:1 (92, 187:1)[b]	61, 7:1
3	I	CO_2Et	87, 96:1	76, 29:1
4	Br	H	68, 6:1	58, 5:1
5	Br	OMe	57, 4:1	35, 1:1

[a]Alk = 3-phenylpropyl. Reactions were assembled in a nitrogen filled glovebox in 1.25 mL of DMA. Yields determined by GC. [b]1.0 equiv of NaI used.

Table 3. L5 Enables the Coupling of Organic Chlorides[a]

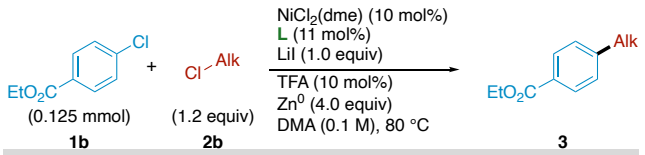

entry	L	yield **3** (%)	selectivity (**3**:**4**)
1	L1	4	1:114
2	L2	11	1:9
3	L5	62	25:1

[a]Alk = 3-Phenylpropyl. Reactions were assembled in a nitrogen filled glovebox in 1.25 mL of DMA. Yields determined by GC.

For example, the low reactivity of organochlorides complicates their activation in XEC reactions. Slow activation of the alkyl chloride can lead to decomposition of the (L)Ni^{II}(Ar)X intermediate and low selectivity. Current methods overcome this obstacle by utilizing specialized ligands or stoichiometric silane reagents.[63,64] We hypothesized that the increased stability of the (L)Ni^{II}(Ar)X intermediate afforded by **L5** may allow for the coupling of unactivated alkyl chlorides. Indeed, by modifying the model reaction conditions, we found that **L5** enables the coupling of an aryl and alkyl chloride in 62% GC yield, while other common bipyridines **L1** and **L2** provide low yield and selectivity (Table 3, Figure S4.10). These results demonstrate that improved bipyridine ligands can expand the accessible pools of coupling partners for bipyridine-nickel catalysts and suggest that more general improvements in scope and yield may be possible.

Table 4. L5 Improves the Selectivity of Decarboxylative XEC[a]

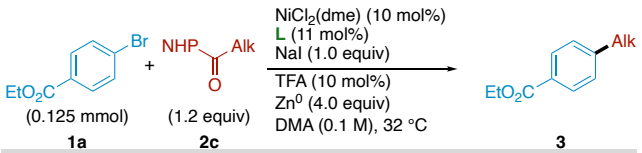

entry	L	yield **3** (%)	selectivity (**3**:**4**)
1	L2	62	25:1
2	L5	68[b]	226:1

[a]Alk = 3-Phenylpropyl. NHP = N-hydroxyphthalimide. Reactions were assembled in a nitrogen filled glovebox in 1.25 mL of DMA. Yields determined by GC. [b]The remaining mass balance was recovered as unreacted **1a**.

Table 5. L5 Increases the Efficiency of *N*-Alkyl Pyridinium Salt XEC and Enables a New Substrate Pairing[a]

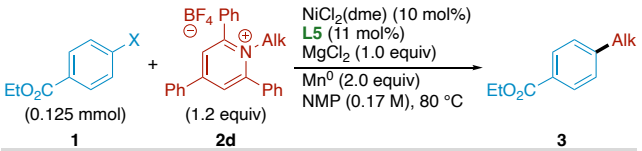

entry	X	yield **3** (%)	selectivity (**3**:**4**)
1	Br	98	84:1
2	Cl	55	7:1
3[b]	Cl	86	8:1

[a]Alk = 3-Phenylpropyl. Reactions were assembled in a nitrogen filled glovebox in 735 µL of NMP. Yields determined by GC. [b]20 mol% of $NiCl_2$(dme) and 22 mol% of **L5** were used.

We found that **L5** enables higher yields than **L2** in the decarboxylative arylation of an *N*-hydroxyphthalimide ester with an aryl bromide (Table 4, Figure S4.12). Notably, the coupling of redox-active esters with bromoarenes often requires the use of carboxamidine-based ligands to enable high conversion and selectivity.[65–67] These results suggest that **L5** may be widely useful in the coupling a variety of electrophiles. Indeed, we were also able to directly substitute **L5** for **L2** in the reported coupling of *N*-alkyl 2,4,6-triphenylpyridiniums with aryl bromides (Table 5).[68] We found that the use of this ligand yielded the desired product in 98% yield (vs 74–85% published yield for similar compounds using **L2**).[68–70] This extended the observed trend in yield from the published optimization in the original report—**L1**<**L2**<**L5**. While arylation of *N*-alkylpyridiniums is well-known for bromoarenes, effective coupling of chloroarenes remains undeveloped.[18] We hypothesized that, in addition to avoiding aryl homodimer, the increased electron-density of **L5** may allow for more rapid oxidative addition into chloroarenes. We found that the equivalent chloroarene coupled in 55% yield using the same conditions and increasing the catalyst loading—leveraging the low rate of aryl dimerization afforded by this catalyst, which should be increased at higher catalyst concentrations—led to an 86% GC yield (Table 4, Figure S.11). Application of these ligands to a variety of XEC reactions and the design of further improved ligands is in process and will be reported in due course.

Overall, this work demonstrates that 4,4'-bis(dialkylamino)-2,2'-bipyridines offer a significant increase in selectivity over the state-of-the-art in bipyridine ligands. Despite the utility of these electron-rich bpy ligands and their presence in the development of novel photocatalysts, we could find only a single use of **L5** for nickel-catalyzed cross-coupling on a particularly challenging substrate.[71–73] We hypothesize that the relatively modest increase in yield when using **L2** in lieu of **L1** in combination with the difficulty in synthesizing novel, electron-rich bipyridines made these ligands an unattractive target for synthetic efforts. This work shows how in silico evaluation can aid in the prioritization of limited resources for maximum success in catalyst development, similar to their routine use in drug development. Currently, only the highest performing catalyst, **L5**, is commercially available for a reasonable price.[74,75] While we found them to be slightly less selective in our benchmark reactions, **L3** and **L4** may offer benefits in solubility and selectivity in specific applications.

Conclusions

In conclusion, we have applied computational and statistical methods to develop a model for selectivity in nickel-catalyzed cross-electrophile coupling. The two resulting models—a binary classification of a ligands' applicability based on the ground state geometry of their (L)Ni^{II}(Ph)Br complex and a linear relationship between the *NPA* charge of the ipso phenyl carbon of the low energy (L)Ni^{II}(Ph)Br complex—enable the prediction of the performance of a variety of substitution patterns with diverse functionalities. This study also highlighted the importance of designing a diverse, informative training set to minimize collinearity in computational parameters, and enhance interpretability. The use of parameters derived from a representative on-cycle intermediate enable strong models and mechanistic insight. These results suggest that, in contrast to previous stoichiometric studies under redox-neutral conditions, the primary dimerization pathway in XEC is not disproportionation of the (L)Ni^{II}(Ar)Br intermediate.

Using our model, we identified a series of improved 4,4'-bis(dialkylamino)-2,2'-bipyridines. These ligands display significant improvements in selectivity and yield compared to the current state-of-the-art bipyridines. Further, they can be easily substituted into other cross electrophile coupling reactions to increase the yield and allow access to more diverse coupling partners. We expect that adoption of these ligands will enable more robust, selective, and widely applicable cross electrophile couplings.

This study provides further evidence of how modern statistical techniques are poised to make a large impact on nickel-catalyzed XEC. Overall, the expanded use of diverse statistical and computational tools will bolster experimental insight and enable more efficient and impactful ligand design and selection. The dataset that we used to generate these models persists and should be applicable to a variety of nickel-catalyzed processes. We have made the entire dataset, including parameters for common and uncommon bipyridines (such as ligands that currently exist only in silico) available as a supplementary spreadsheet. We hope that this dataset will make application of these methods more accessible to other researchers.

ASSOCIATED CONTENT

Supporting Information

The Supporting Information is available free of charge on the ACS Publications website.

Experimental and synthetic procedures, characterization data for all new compounds, computational details, and guide to descriptor spreadsheet (PDF)

Coordinates of all computed structures (XYZ)

Descriptors used for statistical modeling (XLSX)

Experimental data used for initial statistical modeling (XLSX)

Experimental data used for focused statistical modeling (XLSX)

AUTHOR INFORMATION

Corresponding Authors

Matthew S. Sigman – *Department of Chemistry, University of Utah, Salt Lake City, UT 84112, United States;* orcid.org/0000-0002-5746-8830; Email: sigman@chem.utah.edu

Eric C. Hansen – *Chemical Research and Development, Pfizer Worldwide Research and Development, Groton, CT 06340, United States*; orcid.org/0000-0002-5057-4577; Email: eric.hansen@pfizer.com

Daniel J. Weix – *Department of Chemistry, University of Wisconsin-Madison, Madison, WI 53706, United States*; orcid.org/0000-0002-9552-3378; Email: dweix@wisc.edu

Authors

Michelle E. Akana – *Department of Chemistry, University of Wisconsin-Madison, Madison, WI 53706, United States*; orcid.org/0000-0002-1148-7059

Sergei Tcyrulnikov – Chemical Research and Development, Pfizer Worldwide Research and Development, Groton, CT 06340, United States

Brett D. Akana-Schneider – *Department of Chemistry, University of Wisconsin-Madison, Madison, WI 53706, United States*; orcid.org/0000-0002-2249-3809

Giselle P. Reyes – Chemical Research and Development, Pfizer Worldwide Research and Development, Groton, CT 06340, United States

Sebastien Monfette – Chemical Research and Development, Pfizer Worldwide Research and Development, Groton, CT 06340, United States; orcid.org/0000-0002-8394-4423

Author Contributions

The manuscript was written through contributions of all authors. All authors have given approval to the final version of the manuscript.

Notes

The authors declare no competing financial interest. The data that support the findings in this work are available within the paper and Supporting Information.

ACKNOWLEDGMENT

This work was supported by the NSF (CHE-1900366 to DJW and CHE-2154502 to MSS), the University of Wisconsin-Madison (PPG Fellowship to MEA), and Pfizer. NMR and high resolution mass spectrometry results included in this report were recorded at the Paul Bender Chemistry Instrumentation Center, a University of Wisconsin-Madison Department of Chemistry facility. NMR instruments were purchased with the support of the National Science Foundation (CHE-1048642) and a generous gift by Paul J. and Margaret M. Bender. Funds for the high resolution mass spectrometer were obtained from the National Institutes of Health award 1S10OD020022. The calculations used for modeling were performed using computational resources managed and supported by the University of Wisconsin-Madison Department of Chemistry Phoenix cluster and the National Science Foundation award CHE-0840494. We thank Dr. Tobias Gensch, Dr. Ellyn Peters, and Dr. David B. Vogt (University of Utah) for assistance with software packages for statistical analysis.

REFERENCES

(1) Greaves, M. E.; Johnson Humphrey, E. L. B.; Nelson, D. J. Reactions of Nickel(0) with Organochlorides, Organobromides, and Organoiodides: Mechanisms and Structure/Reactivity Relationships. *Catal. Sci. Technol.* **2021**, *11* (9), 2980–2996. DOI: 10.1039/D1CY00374G.

(2) In a continuing series of minireviews of recent advances in nonprecious metal catalysis, bipyridines and related nitrogenous ligands are a stable supporting ligand for nickel catalysts. For the most recent example, see Thane, T. A.; Jarvo, E. R. Ligand-Based Control of Nickel Catalysts: Switching Chemoselectivity from One-Electron to Two-Electron Pathways in Competing Reactions of 4-Halotetrahydropyrans. *Org. Lett.* **2022**, *24* (28), 5003–5008. DOI: 10.1021/acs.orglett.2c01335.

(3) Haibach, M. C.; Shekhar, S.; Ahmed, T. S.; Ickes, A. R. Recent Advances in Nonprecious Metal Catalysis. *Org. Process Res. Dev.* **2023**, *27* (3), 423–447. DOI: 10.1021/acs.oprd.2c00344.

(4) Hamby, T. B.; LaLama, M. J.; Sevov, C. S. Controlling Ni Redox States by Dynamic Ligand Exchange for Electroreductive Csp3–Csp2 Coupling. *Science* **2022**, *376* (6591), 410–416. DOI: 10.1126/science.abo0039.

(5) Richmond, E.; Moran, J. Recent Advances in Nickel Catalysis Enabled by Stoichiometric Metallic Reducing Agents. *Synthesis* **2018**, *50* (03), 499–513. DOI: 10.1055/s-0036-1591853.

(6) Chan, A. Y.; Perry, I. B.; Bissonnette, N. B.; Buksh, B. F.; Edwards, G. A.; Frye, L. I.; Garry, O. L.; Lavagnino, M. N.; Li, B. X.; Liang, Y.; Mao, E.; Millet, A.; Oakley, J. V.; Reed, N. L.; Sakai, H. A.; Seath, C. P.; MacMillan, D. W. C. Metallaphotoredox: The Merger of Photoredox and Transition Metal Catalysis. *Chem. Rev.* **2022**, *122* (2), 1485–1542. DOI: 10.1021/acs.chemrev.1c00383.

(7) Jutand, A. Contribution of Electrochemistry to Organometallic Catalysis. *Chem. Rev.* **2008**, *108* (7), 2300–2347. DOI: 10.1021/cr068072h.

(8) Jose, J.; Diana, E. J.; Kanchana, U. S.; Mathew, T. V. Recent Advances in the Nickel-catalysed Electrochemical Coupling Reactions with a Focus on the Type of Bond Formed. *Asian J. Org. Chem.* **2023**, *12* (2), e202200593 1-20. DOI: 10.1002/ajoc.202200593.

(9) Franke, M. C.; Weix, D. J. Recent Advances in Electrochemical, Ni-Catalyzed C–C Bond Formation. *Isr. J. Chem.* **2023**, e202300089. DOI: 10.1002/ijch.202300089.

(10) Lovering, F.; Bikker, J.; Humblet, C. Escape from Flatland: Increasing Saturation as an Approach to Improving Clinical Success. *J. Med. Chem.* **2009**, *52* (21), 6752–6756. DOI: 10.1021/jm901241e.

(11) Lovering, F. Escape from Flatland 2: Complexity and Promiscuity. *MedChemComm* **2013**, *4* (3), 515. DOI: 10.1039/c2md20347b.

(12) Beutner, G. L.; Simmons, E. M.; Ayers, S.; Bemis, C. Y.; Goldfogel, M. J.; Joe, C. L.; Marshall, J.; Wisniewski, S. R. A Process Chemistry Benchmark for Sp^2–Sp^3 Cross Couplings. *J. Org. Chem.* **2021**, *86* (15), 10380–10396. DOI: 10.1021/acs.joc.1c01073.

(13) Biswas, S.; Weix, D. J. Mechanism and Selectivity in Nickel-Catalyzed Cross-Electrophile Coupling of Aryl Halides with Alkyl Halides. *J. Am. Chem. Soc.* **2013**, *135* (43), 16192–16197. DOI: 10.1021/ja407589e.

(14) Lin, Q.; Spielvogel, E. H.; Diao, T. Carbon-Centered Radical Capture at Nickel(II) Complexes: Spectroscopic Evidence, Rates, and Selectivity. *Chem* **2023**, *9* (5), 1295–1308. DOI: 10.1016/j.chempr.2023.02.010.

(15) Franke, M. C.; Longley, V. R.; Rafiee, M.; Stahl, S. S.; Hansen, E. C.; Weix, D. J. Zinc-Free, Scalable Reductive Cross-Electrophile Coupling

Driven by Electrochemistry in an Undivided Cell. *ACS Catal.* **2022**, *12* (20), 12617–12626. DOI: 10.1021/acscatal.2c03033.

(16) Chi, B. K.; Widness, J. K.; Gilbert, M. M.; Salgueiro, D. C.; Garcia, K. J.; Weix, D. J. In-Situ Bromination Enables Formal Cross-Electrophile Coupling of Alcohols with Aryl and Alkenyl Halides. *ACS Catal.* **2022**, *12* (1), 580–586. DOI: 10.1021/acscatal.1c05208.

(17) Perkins, R. J.; Hughes, A. J.; Weix, D. J.; Hansen, E. C. Metal-Reductant-Free Electrochemical Nickel-Catalyzed Couplings of Aryl and Alkyl Bromides in Acetonitrile. *Org. Process Res. Dev.* **2019**, *23* (8), 1746–1751. DOI: 10.1021/acs.oprd.9b00232.

(18) Fu, J.; Lundy, W.; Chowdhury, R.; Twitty, J. C.; Dinh, L. P.; Sampson, J.; Lam, Y.; Sevov, C. S.; Watson, M. P.; Kalyani, D. Nickel-Catalyzed Electroreductive Coupling of Alkylpyridinium Salts and Aryl Halides. *ACS Catal.* **2023**, *13* (14), 9336–9345. DOI: 10.1021/acscatal.3c01939.

(19) Hofstra, J. L.; Cherney, A. H.; Ordner, C. M.; Reisman, S. E. Synthesis of Enantioenriched Allylic Silanes via Nickel-Catalyzed Reductive Cross-Coupling. *J. Am. Chem. Soc.* **2018**, *140* (1), 139–142. DOI: 10.1021/jacs.7b11707.

(20) Charboneau, D. J.; Barth, E. L.; Hazari, N.; Uehling, M. R.; Zultanski, S. L. A Widely Applicable Dual Catalytic System for Cross-Electrophile Coupling Enabled by Mechanistic Studies. *ACS Catal.* **2020**, *10* (21), 12642–12656. DOI: 10.1021/acscatal.0c03237.

(21) A significant amount of work exists in which a titanium or cobalt co-catalyst is employed to generate an alkyl radical from an electrophile that is unreactive with common nickel-catalysts. However, since these systems rely on the co-catalyst to enable reactivity rather than improve selectivity, we have chosen not to discuss them in this report.

(22) Ackerman-Biegasiewicz, L. K. G.; Kariofillis, S. K.; Weix, D. J. Multimetallic-Catalyzed C–C Bond-Forming Reactions: From Serendipity to Strategy. *J. Am. Chem. Soc.* **2023**, *145* (12), 6596–6614. DOI: 10.1021/jacs.2c08615.

(23) Weix, D. J. Methods and Mechanisms for Cross-Electrophile Coupling of Csp2 Halides with Alkyl Electrophiles. *Acc. Chem. Res.* **2015**, *48* (6), 1767–1775. DOI: 10.1021/acs.accounts.5b00057.

(24) Prieto Kullmer, C. N.; Kautzky, J. A.; Krska, S. W.; Nowak, T.; Dreher, S. D.; MacMillan, D. W. C. Accelerating Reaction Generality and Mechanistic Insight through Additive Mapping. *Science* **2022**, *376* (6592), 532–539. DOI: 10.1126/science.abn1885.

(25) Wang, X.; Wang, S.; Xue, W.; Gong, H. Nickel-Catalyzed Reductive Coupling of Aryl Bromides with Tertiary Alkyl Halides. *J. Am. Chem. Soc.* **2015**, *137* (36), 11562–11565. DOI: 10.1021/jacs.5b06255.

(26) Douthwaite, J. L.; Zhao, R.; Shim, E.; Mahjour, B.; Zimmerman, P. M.; Cernak, T. Formal Cross-Coupling of Amines and Carboxylic Acids to Form Sp^3–Sp^2 Carbon–Carbon Bonds. *J. Am. Chem. Soc.* **2023**, *145* (20), 10930–10937. DOI: 10.1021/jacs.2c11563.

(27) Tang, T.; Hazra, A.; Min, D. S.; Williams, W. L.; Jones, E.; Doyle, A. G.; Sigman, M. S. Interrogating the Mechanistic Features of Ni(I)-Mediated Aryl Iodide Oxidative Addition Using Electroanalytical and Statistical Modeling Techniques. *J. Am. Chem. Soc.* **2023**, jacs.3c01726. DOI: 10.1021/jacs.3c01726.

(28) Kim, Y.; Iwai, T.; Fujii, S.; Ueno, K.; Sawamura, M. Dumbbell-Shaped 2,2′-Bipyridines: Controlled Metal Monochelation and Application to Ni-Catalyzed Cross-Couplings. *Chem. – Eur. J.* **2021**, *27* (7), 2289–2293. DOI: 10.1002/chem.202004053.

(29) Hansen, E. C.; Pedro, D. J.; Wotal, A. C.; Gower, N. J.; Nelson, J. D.; Caron, S.; Weix, D. J. New Ligands for Nickel Catalysis from Diverse Pharmaceutical Heterocycle Libraries. *Nat. Chem.* **2016**, *8* (12), 1126–1130. DOI: 10.1038/nchem.2587.

(30) Isbrandt, E. S.; Sullivan, R. J.; Newman, S. G. High Throughput Strategies for the Discovery and Optimization of Catalytic Reactions. *Angew. Chem. Int. Ed.* **2019**, *58* (22), 7180–7191. DOI: 10.1002/anie.201812534.

(31) Aguirre, A. L.; Loud, N. L.; Johnson, K. A.; Weix, D. J.; Wang, Y. ChemBead Enabled High-Throughput Cross-Electrophile Coupling Reveals a New Complementary Ligand. *Chem. – Eur. J.* **2021**, *27* (51), 12981–12986. DOI: 10.1002/chem.202102347.

(32) *Phosphine Predictor | Sigma-Aldrich*. https://www.sigmaaldrich.com/deepweb/assets/sigmaaldrich/product/documents/377/478/phosphine-predictor-br80087en-ms.pdf (accessed 2023-07-08).

(33) Zhao, S.; Gensch, T.; Murray, B.; Niemeyer, Z. L.; Sigman, M. S.; Biscoe, M. R. Enantiodivergent Pd-Catalyzed C–C Bond Formation Enabled through Ligand Parameterization. *Science* **2018**, *362* (6415), 670–674. DOI: 10.1126/science.aat2299.

(34) Crawford, J. M.; Gensch, T.; Sigman, M. S.; Elward, J. M.; Steves, J. E. Impact of Phosphine Featurization Methods in Process Development. *Org. Process Res. Dev.* **2022**, *26* (4), 1115–1123. DOI: 10.1021/acs.oprd.1c00357.

(35) The related 4,4′-diamino-2,2′-bipyridine has been utilized in a single report of the nickel-catalyzed cross-electrophile coupling of chlorodifluoromethane, see Zhang, C.; Santiago, C. B.; Crawford, J. M.; Sigman, M. S. Enantioselective Dehydrogenative Heck Arylations of Trisubstituted Alkenes with Indoles to Construct Quaternary Stereocenters. *J. Am. Chem. Soc.* **2015**, *137* (50), 15668–15671. DOI: 10.1021/jacs.5b11335.

(36) Guo, J.-Y.; Minko, Y.; Santiago, C. B.; Sigman, M. S. Developing Comprehensive Computational Parameter Sets To Describe the Performance of Pyridine-Oxazoline and Related Ligands. *ACS Catal.* **2017**, *7* (6), 4144–4151. DOI: 10.1021/acscatal.7b00739.

(37) Lau, S. H.; Borden, M. A.; Steiman, T. J.; Wang, L. S.; Parasram, M.; Doyle, A. G. Ni/Photoredox-Catalyzed Enantioselective Cross-Electrophile Coupling of Styrene Oxides with Aryl Iodides. *J. Am. Chem. Soc.* **2021**, *143* (38), 15873–15881. DOI: 10.1021/jacs.1c08105.

(38) Biswas, S.; Qu, B.; Desrosiers, J.-N.; Choi, Y.; Haddad, N.; Yee, N. K.; Song, J. J.; Senanayake, C. H. Nickel-Catalyzed Cross-Electrophile Reductive Couplings of Neopentyl Bromides with Aryl Bromides. *J. Org. Chem.* **2020**, *85* (12), 8214–8220. DOI: 10.1021/acs.joc.0c00549.

(39) Frisch, M. J.; Trucks, G. W.; Schlegel, H. B.; Scuseria, G. E.; Robb, M. A.; Cheeseman, J. R.; Scalmani, G.; Barone, V.; Petersson, G. A.; Nakatsuji, H.; Li, X.; Caricato, M.; Marenich, A. V.; Bloino, J.; Janesko, B. G.; Gomperts, R.; Mennucci, B.; Hratchian, H. P.; Ortiz, J. V.; Izmaylov, A. F.; Sonnenberg, J. L.; Williams; Ding, F.; Lipparini, F.; Egidi, F.; Goings, J.; Peng, B.; Petrone, A.; Henderson, T.; Ranasinghe, D.; Zakrzewski, V. G.; Gao, J.; Rega, N.; Zheng, G.; Liang, W.; Hada, M.; Ehara, M.; Toyota, K.; Fukuda, R.; Hasegawa, J.; Ishida, M.; Nakajima, T.; Honda, Y.; Kitao, O.; Nakai, H.; Vreven, T.; Throssell, K.; Montgomery Jr., J. A.; Peralta, J. E.; Ogliaro, F.; Bearpark, M. J.; Heyd, J. J.; Brothers, E. N.; Kudin, K. N.; Staroverov, V. N.; Keith, T. A.; Kobayashi, R.; Normand, J.; Raghavachari, K.; Rendell, A. P.; Burant, J. C.; Iyengar, S. S.; Tomasi, J.; Cossi, M.; Millam, J. M.; Klene, M.; Adamo, C.; Cammi, R.; Ochterski, J. W.; Martin, R. L.; Morokuma, K.; Farkas, O.; Foresman, J. B.; Fox, D. J. Gaussian 16 Rev. C.01, 2016.

(40) Zhao, Y.; Truhlar, D. G. The M06 Suite of Density Functionals for Main Group Thermochemistry, Thermochemical Kinetics, Noncovalent Interactions, Excited States, and Transition Elements: Two New Functionals and Systematic Testing of Four M06-Class Functionals and 12 Other Functionals. *Theor. Chem. Acc.* **2008**, *120* (1), 215–241. DOI: 10.1007/s00214-007-0310-x.

(41) Dunning, T. H. Gaussian Basis Sets for Use in Correlated Molecular Calculations. I. The Atoms Boron through Neon and Hydrogen. *J. Chem. Phys.* **1989**, *90*, 1007–1023. DOI: 10.1063/1.456153.

(42) Wilson, A. K.; Woon, D. E.; Peterson, K. A.; Dunning, T. H. Gaussian Basis Sets for Use in Correlated Molecular Calculations. IX. The Atoms Gallium through Krypton. *J. Chem. Phys.* **1999**, *110*, 7667–7676. DOI: 10.1063/1.478678.

(43) Hay, P. J.; Wadt, W. R. Ab Initio Effective Core Potentials for Molecular Calculations. Potentials for the Transition Metal Atoms Sc to Hg. *J. Chem. Phys.* **1985**, *82* (1), 270–283. DOI: 10.1063/1.448799.

(44) Dolg, M.; Wedig, U.; Stoll, H.; Preuss, H. Energy-adjusted Ab Initio Pseudopotentials for the First Row Transition Elements. *J. Chem. Phys.* **1987**, *86* (2), 866–872. DOI: 10.1063/1.452288.

(45) Marenich, A. V.; Cramer, C. J.; Truhlar, D. G. Universal Solvation Model Based on Solute Electron Density and on a Continuum Model of the Solvent Defined by the Bulk Dielectric Constant and Atomic Surface Tensions. *J. Phys. Chem. B* **2009**, *113* (18), 6378–6396. DOI: 10.1021/jp810292n.

(46) Glendening, E. D.; Badenhoop, J. K.; Reed, A. E.; Carpenter, J. E.; Bohmann, J. A.; Morales, C. M.; Karafiloglou, P.; Landis, C. R.; Weinhold, F. NBO 7.0.10, 2018.

(47) UM06/cc-pVDZ,SDD(Ni)//UM06/cc-pVDZ,LANL2DZ(Ni), SMD: N,N-dimethylacetamide in Gaussian 16, rev. C.01. .

(48) Yuan, M.; Song, Z.; Badir, S. O.; Molander, G. A.; Gutierrez, O. On the Nature of C(Sp3)–C(Sp2) Bond Formation in Nickel-Catalyzed Tertiary Radical Cross-Couplings: A Case Study of Ni/Photoredox Catalytic Cross-Coupling of Alkyl Radicals and Aryl Halides. *J. Am. Chem. Soc.* **2020**, *142* (15), 7225–7234. DOI: 10.1021/jacs.0c02355.

(49) Newman-Stonebraker, S. H.; Smith, S. R.; Borowski, J. E.; Peters, E.; Gensch, T.; Johnson, H. C.; Sigman, M. S.; Doyle, A. G. Univariate Classification of Phosphine Ligation State and Reactivity in Cross-Coupling Catalysis. *Science* **2021**, *374* (6565), 301–308. DOI: 10.1126/science.abj4213.

(50) Janssen-Müller, D.; Sahoo, B.; Sun, S.; Martin, R. Tackling Remote Sp^3 C–H Functionalization via Ni-Catalyzed "Chain-walking" Reactions. *Isr. J. Chem.* **2020**, *60* (3–4), 195–206. DOI: 10.1002/ijch.201900072.

(51) Rago, A. J.; Vasilopoulos, A.; Dombrowski, A. W.; Wang, Y. Di(2-Picolyl)Amines as Modular and Robust Ligands for Nickel-Catalyzed C(Sp^2)–C(Sp^3) Cross-Electrophile Coupling. *Org. Lett.* **2022**, *24* (46), 8487–8492. DOI: 10.1021/acs.orglett.2c03346.

(52) While the most electron-poor pyridine is consistently trans to the phenyl ligand in the low-energy square planar isomer, the difference in energy in the two isomers (< 0.5 kcal/mol), and relatively low energy to access a tetrahedral geometry, suggest that both isomers form and are interconverting in solution. As such, we cannot clearly determine if the observed trend in donation is attributable to the reactivity of the phenyl ligand or the bromide; however, our hypothesis concerning degradative reduction to form (L)Ni^I(Ar) suggests that the high energy isomer may play a key role.

(53) While selectivity is determined by the least donating pyridine unit, we did observe improved catalyst stability and a decrease in desbromination when an electron-donating group was incorporated. We hypothesize that these mixed-donicity bipyridines may have utility in the coupling of acyl electrophiles or in mixed biaryl synthesis.

(54) Yamamoto, T.; Wakabayashi, S.; Osakada, K. Mechanism of C–C Coupling Reactions of Aromatic Halides, Promoted by Ni(COD)2 in the Presence of 2,2′-Bipyridine and PPh3, to Give Biaryls. *J. Organomet. Chem.* **1992**, *428* (1–2), 223–237. DOI: 10.1016/0022-328X(92)83232-7.

(55) Olivares, A. M.; Weix, D. J. Multimetallic Ni- and Pd-Catalyzed Cross-Electrophile Coupling To Form Highly Substituted 1,3-Dienes. *J. Am. Chem. Soc.* **2018**, *140* (7), 2446–2449. DOI: 10.1021/jacs.7b13601.

(56) Kang, K.; Huang, L.; Weix, D. J. Sulfonate Versus Sulfonate: Nickel and Palladium Multimetallic Cross-Electrophile Coupling of Aryl Triflates with Aryl Tosylates. *J. Am. Chem. Soc.* **2020**, *142* (24), 10634–10640. DOI: 10.1021/jacs.0c04670.

(57) Amatore, C.; Jutand, A. Rates and Mechanism of Biphenyl Synthesis Catalyzed by Electrogenerated Coordinatively Unsaturated Nickel Complexes. *Organometallics* **1988**, *7* (10), 2203–2214. DOI: 10.1021/om00100a019.

(58) Colon, I.; Kelsey, D. R. Coupling of Aryl Chlorides by Nickel and Reducing Metals. *J. Org. Chem.* **1986**, *51* (14), 2627–2637. DOI: 10.1021/jo00364a002.

(59) Durandetti, M.; Devaud, M.; Perichon, J. Investigation of the Reductive Coupling of Aryl Halides and/or Ethylchloroacetate Electrocatalyzed by the Precursor NiX2(Bpy) with X(-)=Cl-, Br-, or MeSO3- and Bpy Equals 2,2'-Dipyridyl. *New J. Chem.* **1996**, *20*, 659–667.

(60) We found that electron-rich arenes dimerize more rapidly than electron-poor substrates (Figure S4.8). While this aligns with the results published by Osakada and co-workers, the trend in electron-density of the *ipso* carbon does not extend to our findings concerning the effect of ligand donicity as seen in Figures 2 and 4. Further, the impact of zinc salts (Figure S4.9) and iodide (Figure S4.6) on selectivity indicate that direct disproportionation between two arylnickel(II) species is most likely not the operative mechanism by which **4** forms under these conditions.

(61) We found that decreasing the catalyst loading increases selectivity (Figure S4.7). This suggests that the mechanism by which **4** forms is bimetallic, or displays higher order kinetics than the productive pathway. Since the rate of sequential oxidative addition should have a first order dependence on the concentration of nickel, selectivity would be independent of the catalyst loading of this was the major pathway by which **4** forms.

(62) Based on the observation that selectivity decreases as reactions progress, we hypothesized that zinc(II) salts formed as a byproduct of the reaction promote dimerization. Indeed, we found that adding stoichiometric zinc salts significantly decreases the efficiency of **L5** in the model reaction (Figure S4.7). It is currently unclear if **4** forms via a transient organozinc intermediate, or if bridging zinc intermediates accelerate decomposition of arylnickel(II) complexes.

(63) Kim, S.; Goldfogel, M. J.; Gilbert, M. M.; Weix, D. J. Nickel-Catalyzed Cross-Electrophile Coupling of Aryl Chlorides with Primary Alkyl Chlorides. *J. Am. Chem. Soc.* **2020**, *142* (22), 9902–9907. DOI: 10.1021/jacs.0c02673.

(64) Sakai, H. A.; Liu, W.; Le, C. "Chip"; MacMillan, D. W. C. Cross-Electrophile Coupling of Unactivated Alkyl Chlorides. *J. Am. Chem. Soc.* **2020**, *142* (27), 11691–11697. DOI: 10.1021/jacs.0c04812.

(65) Watanabe, E.; Chen, Y.; May, O.; Ley, S. V. A Practical Method for Continuous Production of sp3-Rich Compounds from (Hetero)Aryl Halides and Redox-Active Esters. *Chem. – Eur. J.* **2020**, *26* (1), 186–191. DOI: 10.1002/chem.201905048.

(66) Salgueiro, D. C.; Chi, B. K.; Guzei, I. A.; García-Reynaga, P.; Weix, D. J. Control of Redox-Active Ester Reactivity Enables a General Cross-Electrophile Approach to Access Arylated Strained Rings**. *Angew. Chem.* **2022**, *134* (33), e202205673. DOI: 10.1002/ange.202205673.

(67) DeCicco, E. M.; Berritt, S.; Knauber, T.; Coffey, S. B.; Hou, J.; Dowling, M. S. Decarboxylative Cross-Electrophile Coupling of (Hetero)Aromatic Bromides and NHP Esters. *J. Org. Chem.* **2023**, *88* (17), 12329–12340. DOI: 10.1021/acs.joc.3c01072.

(68) Liao, J.; Basch, C. H.; Hoerrner, M. E.; Talley, M. R.; Boscoe, B. P.; Tucker, J. W.; Garnsey, M. R.; Watson, M. P. Deaminative Reductive Cross-Electrophile Couplings of Alkylpyridinium Salts and Aryl Bromides. *Org. Lett.* **2019**, *21* (8), 2941–2946. DOI: 10.1021/acs.orglett.9b01014.

(69) Martin-Montero, R.; Yatham, V. R.; Yin, H.; Davies, J.; Martin, R. Ni-Catalyzed Reductive Deaminative Arylation at Sp^3 Carbon Centers. *Org. Lett.* **2019**, *21* (8), 2947–2951. DOI: 10.1021/acs.orglett.9b01016.

(70) We recognize that direct comparison of GC and isolated yields for different compounds is inexact; however, this comparison does provide some insight into the ability to substitute this ligand into published methods.

(71) Escobar, R. A.; Johannes, J. W. A Unified and Practical Method for Carbon–Heteroatom Cross-Coupling Using Nickel/Photo Dual Catalysis. *Chem. – Eur. J.* **2020**, *26* (23), 5168–5173. DOI: 10.1002/chem.202000052.

(72) Gavryushin, A.; Kofink, C.; Manolikakes, G.; Knochel, P. An Efficient Negishi Cross-Coupling Reaction Catalyzed by Nickel(II) and Diethyl Phosphite. *Tetrahedron* **2006**, *62* (32), 7521–7533. DOI: 10.1016/j.tet.2006.03.123.

(73) Xu, C.; Guo, W.-H.; He, X.; Guo, Y.-L.; Zhang, X.-Y.; Zhang, X. Difluoromethylation of (Hetero)Aryl Chlorides with Chlorodifluoromethane Catalyzed by Nickel. *Nat. Commun.* **2018**, *9* (1), 1170. DOI: 10.1038/s41467-018-03532-1.

(74) At the time of writing, **L5** is in stock at Ambeed for $118/g. **L5** is also accessible in two linear steps (50% total yield) from DMAP. **L4** is listed by AstaTech for $106/g, though it is currently backordered. A search of the eMolecules database for **L3** yielded no commercial vendors.

(75) Pinyou, P.; Ruff, A.; Pöller, S.; Ma, S.; Ludwig, R.; Schuhmann, W. Design of an Os Complex-Modified Hydrogel with Optimized Redox Potential for Biosensors and Biofuel Cells. *Chem. – Eur. J.* **2016**, *22* (15), 5319–5326. DOI: 10.1002/chem.201504591.

Insert Table of Contents artwork here